Factor VIIa and the extracellular domains of human tissue factor form a compact complex: a study by X-ray and neutron solution scattering

Alun W. Ashton[a], Geoffrey Kemball-Cook[b], Daniel J.D. Johnson[b], David M.A. Martin[b], Donogh P. O'Brien[b,**], Edward G.D. Tuddenham[b], Stephen J. Perkins[a,*]

[a]*Department of Biochemistry and Molecular Biology, Royal Free Hospital School of Medicine, Rowland Hill Street, London NW3 2PF, UK*
[b]*Haemostasis Research Group, MRC Clinical Sciences Centre, Royal Postgraduate Medical School, Hammersmith Hospital, Du Cane Road, London W12 0NN, UK*

Received 13 September 1995

Abstract The four-domain structure of human factor VIIa and the two-domain structure of tissue factor form a tight complex to initiate blood coagulation. By solution scattering, the mean X-ray and neutron radii of gyration R_G (which determine macromolecular elongation) were found to be 3.25 nm, 2.13 nm and 3.14 nm (± 0.13 nm) for factor VIIa, the extracellular region of tissue factor and their complex in that order. The mean cross-sectional radii of gyration R_{XS} were 1.33 nm, 0.56 nm and 1.42 nm (± 0.13 nm) in that order. The mean lengths were 10.3 nm, 7.7 nm and 10.2 nm in that order. The data show that, in solution, the free proteins have extended domain structures, and the complex is formed by a compact side-by-side alignment of the two proteins along their long axes. The high binding affinity of tissue factor for factor VIIa may thus be accounted for by the occurrence of many intermolecular contacts in the complex.

Key words: Factor VIIa; Tissue factor; Protein structure; Coagulation; X-ray scattering; Neutron scattering

1. Introduction

Blood coagulation has long been recognised as an important process essential for survival. Inappropriate coagulation obstructing blood vessels (or thrombosis) is responsible for much morbidity and mortality. Thrombotic disorders are often associated with cardiovascular, infectious and neoplastic disease. An understanding of the molecular basis of the procoagulant pathways will in the long term help to treat and even prevent many of these thrombotic disorders. Exposure of the membrane-bound receptor, tissue factor, to plasma initiates the coagulation pathways. Upon cell-surface expression of tissue factor, it forms a very stable catalytic enzyme-cofactor complex with the plasma serine protease coagulation factor VIIa (FVIIa) with a K_d of binding estimated to be from 3 pM to 5 nM [1,2].

Both tissue factor and FVIIa are multidomain proteins. The crystal structure for the soluble extracellular region of tissue factor (sTF) [3,4] shows that this contains two C2-type immunoglobulin fold domains. FVIIa contains four domains. The serine protease (SP) and epidermal growth factor (EGF-2) domains in the crystal structure of human factor Xa [5] are highly homologous in primary structure to those found in FVIIa. The NMR structures of the EGF-1 domain of human factors IX and X [6,7] provide a close model for the EGF-1 domain in FVIIa. Finally the known crystal structure of the N-terminal Gla domain of prothrombin [8] may be used as a model for that in FVIIa. While an atomic model for FVIIa can be proposed, there is no information on the relative spatial arrangement of its four domains. In addition, no data is available for the structure of the FVIIa-sTF complex.

Neutron and X-ray scattering studies provide the means, not only for determining the domain orientation of FVIIa, and verifying that for sTF, but also for determining a low resolution structure of the enzyme-cofactor complex [9,10]. A complete set of neutron and X-ray data is reported which characterise the radius of gyration of the overall structure R_G and its cross-section R_{XS}, and the distance distribution function $P(r)$. We show that the FVIIa–sTF complex possesses a compact structure. This offers an explanation for the high affinity of the two proteins for each other in the complex in terms of the ability of many residues, identified from biochemical studies, to form specific intermolecular interactions in the complex.

2. Materials and methods

2.1. Preparations of factor VIIa, tissue factor and their complex

Recombinant wild-type human FVII was expressed in CHO cells [11] and purified to homogeneity by monoclonal antibody affinity chromatography [12] or with final purification carried out using a Resource Q ion-exchange column (Pharmacia, St Albans, UK). FVIIa was derived by autoactivation at 2–4 mg/ml in TBS-Ca buffer (50 mM Tris/150 mM NaCl/5 mM $CaCl_2$ pH 7.4) at room temperature for 18 h, covalently inactivated at the active site by treatment with dansyl-Glu-Gly-Arg-chloromethyl ketone (DEGR-CK, Calbiochem), followed by rechromatography on Mono Q (Pharmacia) to isolate pure FVIIa. Shortly prior to data collection, FVIIa was subjected to gel-filtration on Superose 12 (Pharmacia) in TBS-Ca to remove trace aggregates, then reconcentrated using Centricon-30 devices (Amicon, Stonehouse, UK). In one experiment, purified non-activated FVII was prepared in TBS without prior autoactivation, and was found to be fully activated after data collection. Control experiments indicated that autoactivation is rapid in concentrated solutions of FVII.

Recombinant sTF (residues 1–219) was isolated from *E. coli* cell paste and purified as described previously [13], or alternatively by sequential ion-exchange chromatography on SP Sepharose High Performance and Resource Q columns (Pharmacia). The resulting protein was subjected to gel filtration as above before final reconcentration using Centricon-10 devices (Amicon) prior to data collection.

The complex was formed from FVIIa and sTF, which were purified

*Corresponding author. Fax: (44) (171) 794-9645.
E-mail: steve@rfhsm.ac.uk

**Present address:* Cardiovascular Department, Synthélabo Recherche, 31 Avenue Paul Vaillant Couturier, 92220 Bagneux, France.

Abbreviations: FVIIa, factor VIIa; sTF, soluble extracellular tissue factor (residues 1–219); SP, serine protease; EGF, epidermal growth factor.

SSDI 0014-5793(95)01093-9

as above, concentrated to volumes of 500 μl each, then mixed in TBS-Ca at 37°C for 5 min in a molar ratio of FVIIa : sTF of approximately 1 : 2 as determined by the absorbance at 280 nm. The sTF–FVIIa complex was separated from excess sTF by gel filtration on Superose 12. Fractions from an elution peak corresponding to the complex were pooled and concentrated. sTF was eluted in a later peak as demonstrated by SDS-PAGE analysis [14]. Concentrations c were calculated from calculated absorbance measurements at 280 nm using absorption coefficients (1%, 1 cm) of 12.8, 15.6 and 13.7 for FVIIa, sTF and their complex, respectively [15]. Sequences and carbohydrate contents were obtained from refs. [16–20].

Scattering data were obtained using TBS-Ca buffer in H_2O buffers for X-ray work, while the neutron work involved dialysis at 6°C into the corresponding buffer in ^2H_2O for at least 36 h with four buffer changes. SDS-PAGE under non-reducing conditions before and after scattering was used to verify the integrity of the samples. Samples were stored at 4–6°C until required. X-ray and neutron data collection was performed at 15°C using thermostatted sample holders.

2.2. X-ray and neutron data collection

X-ray curves were obtained in two beam sessions on cameras at Stations 2.1 and 8.2, both equipped with a quadrant detector, at the Synchrotron Radiation Source at Daresbury [21]. Sample-detector distances of 3.14 m and 3.46 m were used, with beam currents of 136 mA to 203 mA and a storage ring energy of 2.0 GeV. This setup resulted in an available Q range of between 0.06 to 2.38 nm^{-1} ($Q = 4\pi \sin\theta/\lambda$; scattering angle = 2θ; wavelength = λ). Samples were measured in Teflon cells with 15–20 μm thick mica windows. Data were recorded using 10 time frames to monitor possible radiation damage effects. Other details of instrument calibration and data reduction are described elsewhere (e.g. in [22]).

Neutron data were obtained during three beam sessions on the LOQ scattering instrument at the ISIS facility at the Rutherford Appleton Laboratory, Didcot, UK [23]. The pulsed neutron beam was derived from bombardment of a tantalum or depleted uranium target by 170–185 μA proton beam currents. A ^{3}He ORDELA wire detector was employed at a sample-to-detector distance of 4.3 m, and yielded an available Q range of 0.05–2.2 nm^{-1}. Samples were measured in 2 mm-thick rectangular quartz Hellma cells. Other details are described elsewhere (e.g. in [22,24]).

2.3. Analysis of reduced X-ray and neutron data

In a given protein-buffer scattering contrast, the radius of gyration R_G is a measure of structural elongation if the internal inhomogeneity of scattering densities within the glycoprotein can be neglected. Analyses of the $I(Q)$ curves at small Q in Guinier plots give the R_G and the forward scattering at zero scattering angle $I(0)$ [25]:

$$\ln I(Q) = \ln I(0) - R_G^2 Q^2/3.$$

The relative values of $I(0)/c$ (c = sample concentration) gives relative molecular weights M_r of the proteins as a control of the data [26]. If the structure is sufficiently elongated, the averaged radius of gyration of the cross-sectional structure R_{XS} and the averaged cross-sectional intensity at zero angle $[I(Q)\cdot Q]_{Q\to 0}$ are obtained from [25,27]:

$$\ln [I(Q)\cdot Q] = \ln [I(Q)\cdot Q]_{Q\to 0} - R_{XS}^2 Q^2/2.$$

The R_G and R_{XS} analyses lead to estimates of triaxial dimensions, where in particular the length of the longest axis $L = [12(R_G^2 - R_{XS}^2)]^{1/2}$ or $L = \pi I(0)/[I(Q)\cdot Q]_{Q\to 0}$ [25,28].

Indirect transformation of the full scattering data in reciprocal space $I(Q)$ into that in real space $P(r)$ was carried out using the GNOM program of Svergun [29].

$$P(r) = \frac{1}{2\pi^2}\int_0^\infty I(Q)\cdot Qr\cdot \sin(Qr)\cdot dQ$$

$P(r)$ corresponds to the distribution of distances r between any two volume elements within one particle. This offers an alternative calculation of R_G and $I(0)$, and gives the maximum dimension of the macromolecule L. To calculate the $P(r)$ curves, the X-ray $I(Q)$ curves contained 350–390 data points extending out to 2.2 nm^{-1} and the neutron $I(Q)$ curves contained 69 data points extending out to 2.1 nm^{-1}. D_{max} was varied in 1 nm steps between 5–20 nm to test the stability of the $P(r)$ transformation. L was determined from the value of r when $P(r)$ became zero at large r; however, errors in L can be significant for reason of the low intensity of $P(r)$ in this region.

3. Results

3.1. Synchrotron X-ray data on factor VIIa, extracellular tissue factor and their complex

The full X-ray scattering curves $I(Q)$ of FVIIa, sTF and their complex were analysed in two distinct Q ranges at low Q in order to obtain the radius of gyration R_G and the cross-sectional radius of gyration R_{XS}. Figs. 1 and 2 show that the final R_G and R_{XS} data were obtained from linear plots in satisfactory QR_G and QR_{XS} ranges. For FVIIa, noticeable radiation damage effects were observed at low Q through apparent aggregate formation. These were analysed using data collected in 10 consecutive 1 min time frames. The R_G and $I(0)$ parameters were stable for the first 2 min of data collection, then increased linearly with time for the remaining 8 min. X-ray data for FVIIa in Figs. 1–3 were analysed using only the first 1 min time-frame. Analyses of the dilution series between 0.6–2.5 mg FVIIa/ml showed no concentration dependence of the R_G or $I(0)/c$ values (c: sample concentration). sTF was stable in the X-ray beam and the entire 10 min data acquisition with 0.9 mg sTF/ml was used for Guinier analyses. The complex (3.9 mg/ml) exhibited slight radiation damage, and the first three time-frames only were used for all data analyses.

The mean X-ray R_G value of FVIIa which defines its overall elongation is 3.24 ± 0.08 nm (Table 1). The R_G/R_O ratio indicates the anisotropy or the degree of elongation of the structure, where R_O is the R_G of the sphere with the same hydrated volume as the protein in question. The R_G/R_O ratio is 1.53 ± 0.04 for FVIIa, which is slightly higher than the averaged value of 1.28 ± 0.10 for single-domain globular proteins [9]. The overall solution structure of FVIIa is thus extended. Its mean R_{XS} value was 1.53 ± 0.13 nm. Calculation of the length L of FVIIa by two methods from the Guinier analyses (section 2) suggests a value of L between 9.9 nm to 11.4 nm. The mean X-ray R_G of sTF was determined to be 1.99 ± 0.05 nm, and resulted in an R_G/R_O ratio of 1.19 ± 0.03. Its mean R_{XS} value is 0.52 nm, and its length L is 6.7 to 7.6 nm. The mean R_G of the complex was 3.20 ± 0.02 nm, its R_G/R_O ratio was 1.33 ± 0.01, its mean R_{XS} value was 1.56 ± 0.02 nm, and its length L was between 9.7 nm to 11.2 nm. The structural anisotropy of the complex was therefore intermediate between those of FVIIa and sTF. However sedimentation data have suggested that the frictional ratio f/f_0 of the complex is 1.52, which is larger than that for FVIIa of 1.39, and implies that the complex is more elongated than FVIIa [30].

The distance distribution function $P(r)$ allows the determination of the maximum dimension L (section 2). The R_G and $I(0)$ parameters calculated from $P(r)$ were all in good agreement with the Guinier analyses (Table 1). The X-ray $P(r)$ curve for FVIIa reached a maximum at r = 3.0 nm to correspond to the most frequently occurring distance within FVIIa. The maxima for sTF and the complex were at 1.2 nm and 3.0 nm. L was determined to be 10 ± 2 nm for FVIIa, 8.0 ± 0.1 nm for sTF and 10.2 ± 0.3 nm for the complex. These were in agreement with the Guinier length calculations (Table 1). It is concluded that the length of the longest axis of the complex is similar to

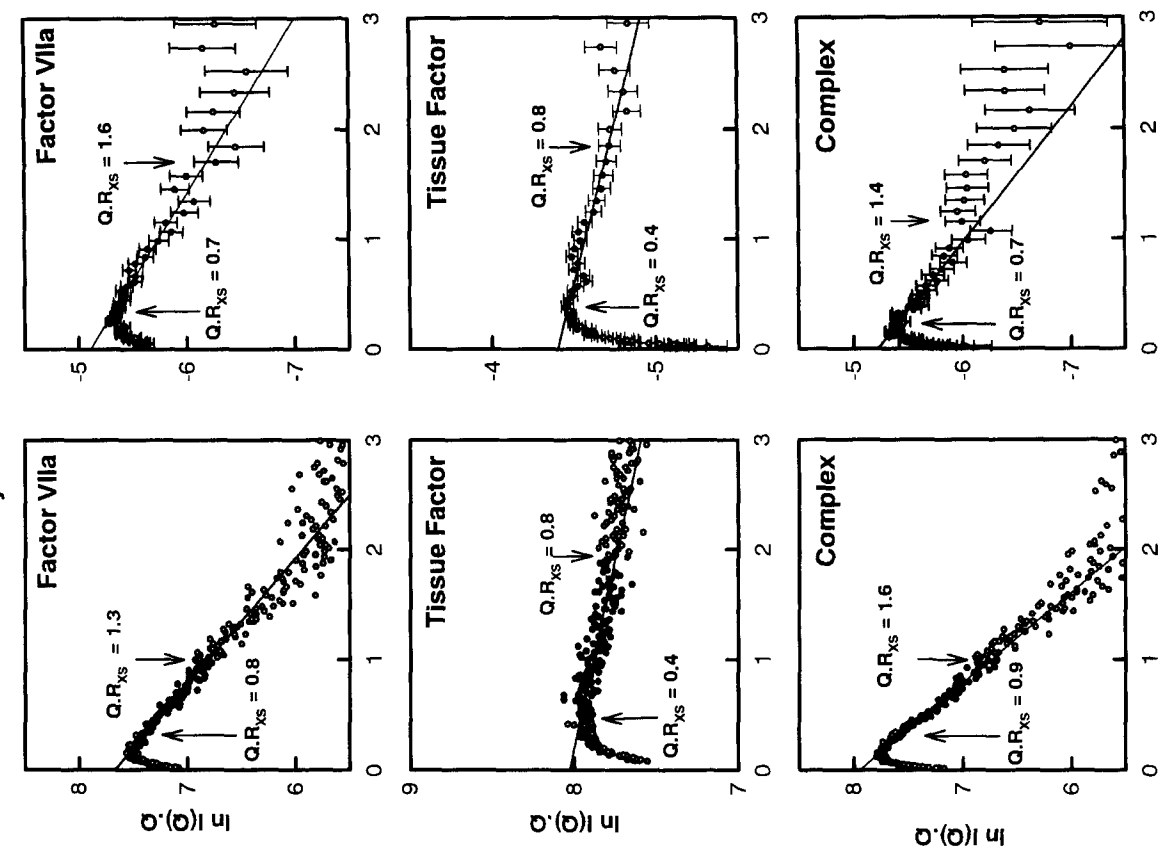

Fig. 2. X-ray and neutron Guinier R_{XS} plots for factor VIIa, extracellular tissue factor and their complex. The scattering curves are the same as in Fig. 1. The filled circles between the $Q \cdot R_{XS}$ ranges as arrowed show the data points used to determine the R_{XS} values (Table 1).

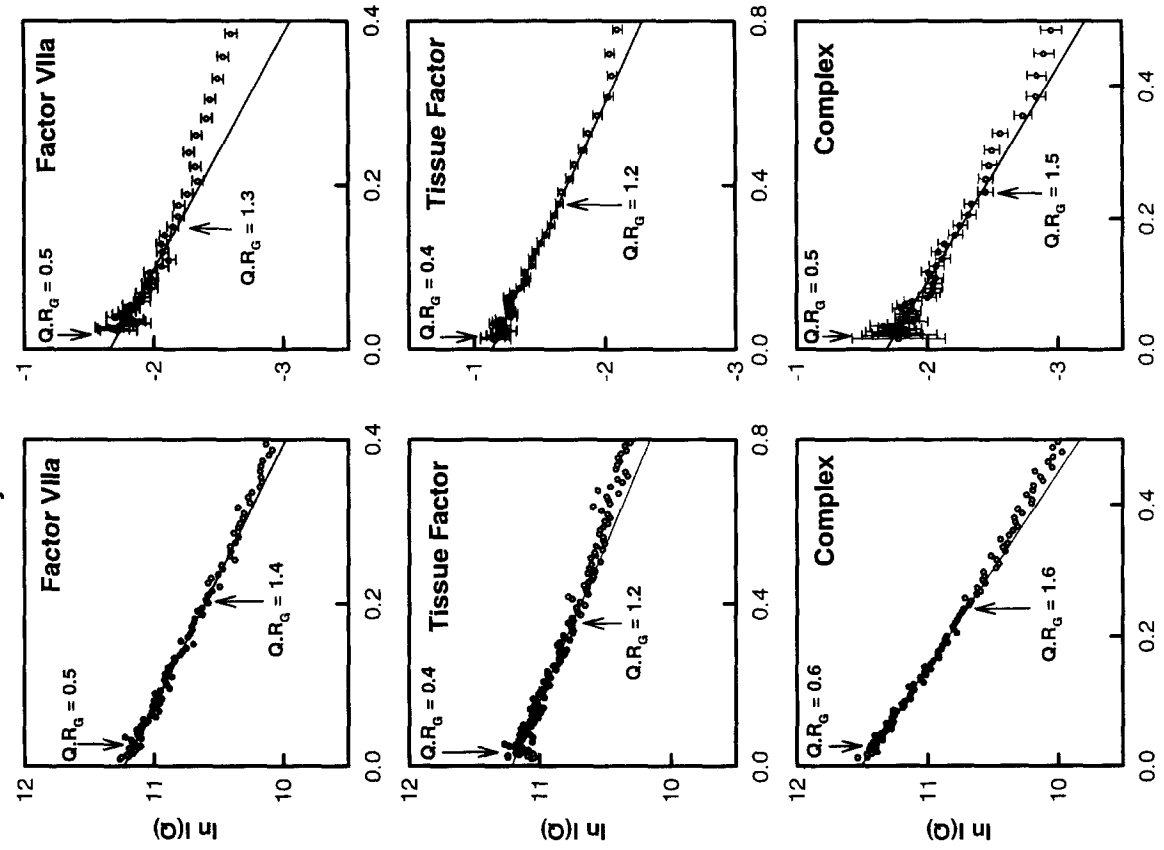

Fig. 1. X-ray and neutron Guinier R_G plots for factor VIIa, extracellular tissue factor and their complex. Values of c for FVIIa were 1.9 and 3.9 mg/ml, those for sTF were 0.9 and 0.9 mg/ml, and those for the complex were 3.9 and 2.6 mg/ml, for X-rays and neutrons, respectively. Filled circles between the $Q \cdot R_G$ ranges show the data points used to determine the R_G values (Table 1).

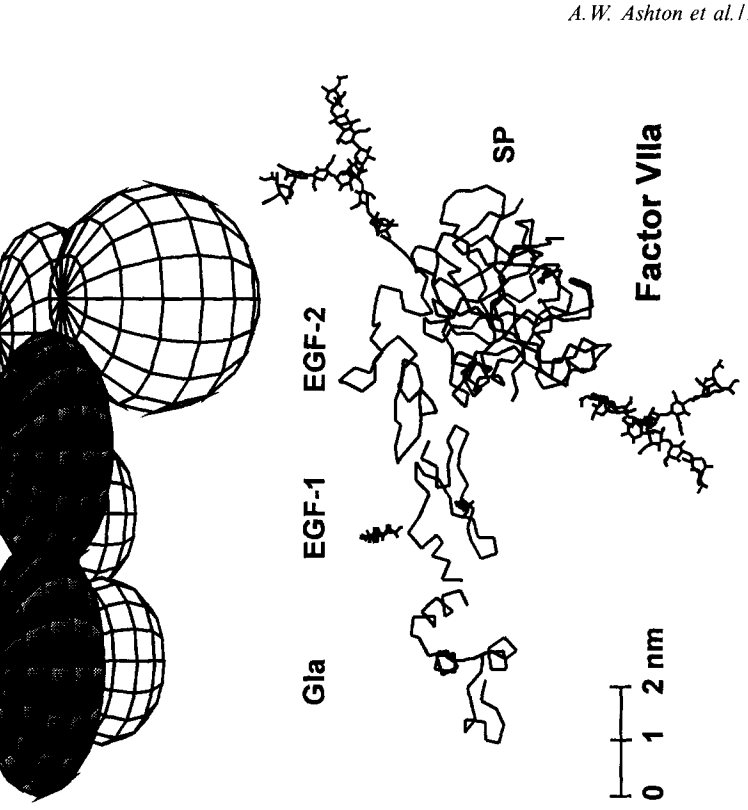

Fig. 4. Schematic diagram of the domains in human factor VIIa and extracellular tissue factor and a possible association in their complex. Upper: sTF has two C2-type immunoglobulin fold domains (residues 1–101 and 108–219), joined by a six-residue linker region [3,4]. *N*-glycosylation sites occur at Asn^{11}, Asn^{124} and Asn^{137}, however the sTF used here was expressed in *E. coli* and hence was not glycosylated. Centre: Schematic ellipsoidal models to represent a possible association of sTF (shaded) and FVIIa to form a compact complex. Lower: FVIIa consists of an N-terminal γ-carboxyglutamic acid (Gla) domain (residues 1–45), followed by two epidermal growth factor (EGF-1 and EGF-2) domains (residues 49–82 and 90–128) and a serine protease (SP) domain (residues 153–406). The Brookhaven codes are 2pfl, 1ixa and 1hcg respectively. N-linked glycosylation sites occur at Asn^{145} and Asn^{322} in SP [18] and O-linked glycosylation sites occur at Ser^{52} and Ser^{60} in EGF-1 [19,20]. It is stressed that the extended rotational orientation between the Gla, EGF-1 and EGF-2 domains in FVIIa is arbitrary.

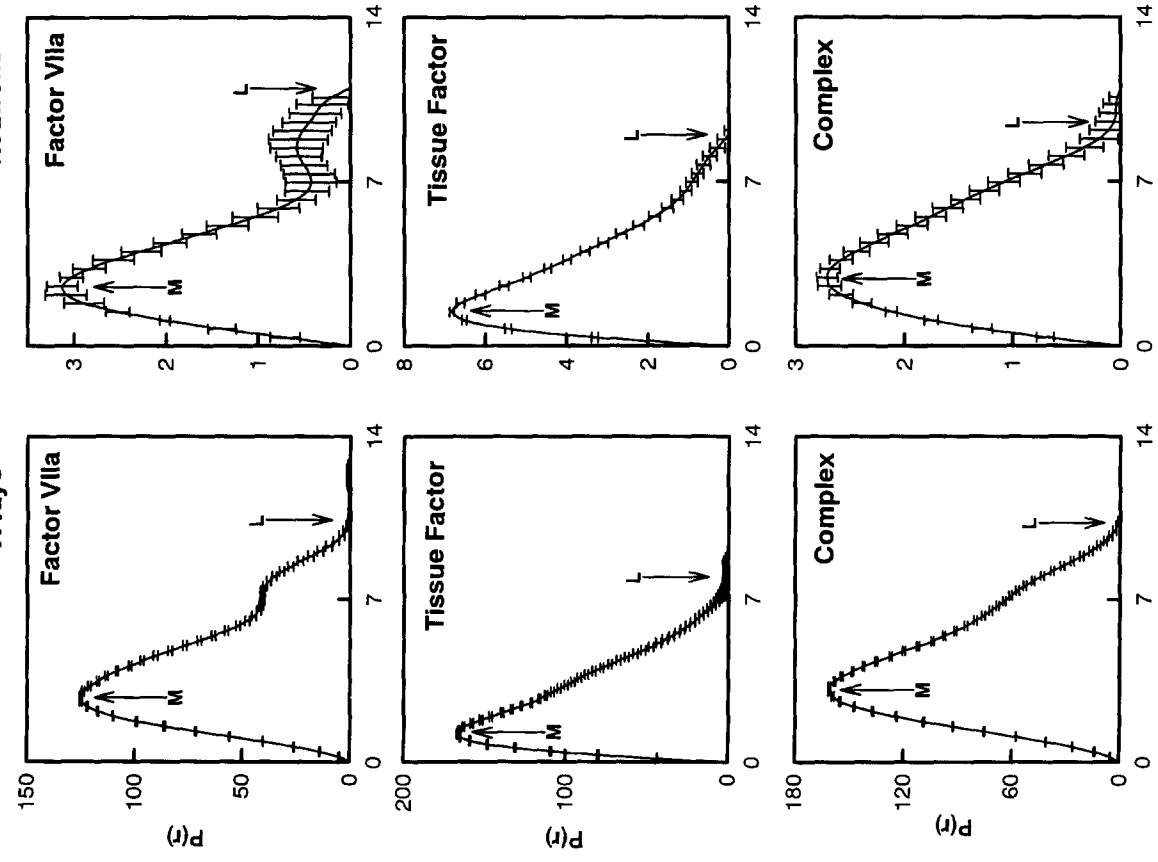

Fig. 3. Distance distribution functions $P(r)$ for factor VIIa, extracellular tissue factor and their complex. The scattering curves are the same as in Fig. 1. The maximum of the $P(r)$ curve is denoted M, the most frequently occurring distance within the protein (Table 1). The maximum dimension is denoted L.

Table 1
Summary of solution scattering data for factor VIIa, extracellular tissue factor and their complex

Guinier analysis	Q ranges used in Guinier fits (nm^{-1}) R_G (nm)	R_{XS} (nm)	L (nm):R_G L (nm):$I(0)$	
P(r) analysis	R_G (nm)		L (nm)	M (nm)
Factor VIIa				
	0.20–0.42	0.6–1.4		
X-ray (7)[1]	3.24 ± 0.08	1.53 ± 0.13	9.9 ± 0.2 11.4 ± 0.5	
	3.37 ± 0.05		10 ± 2	3.0 ± 0.3
Neutron (3)	3.22 ± 0.02	1.13 ± 0.03	10.4 ± 0.1 10.0 ± 1.0	
	3.18 ± 0.05		10 ± 2	2.5 ± 0.1
Tissue factor				
	0.18–0.60	0.7–1.4		
X-ray (4)	1.99 ± 0.05	0.52 ± 0.01	6.7 ± 0.2 7.6 ± 0.3	
	2.12 ± 0.12		8.0 ± 0.1	1.2 ± 0.1
Neutron (1)	2.08 ± 0.04	0.59 ± 0.03	6.9 ± 0.2 8.2 ± 0.1	
	2.32 ± 0.13		9.0	1.6
Complex				
	0.15–0.49	0.6–1.0		
X-ray (2)	3.20 ± 0.02	1.56 ± 0.02	9.7 ± 0.1 11.2 ± 0.1	
	3.23 ± 0.03		10.2 ± 0.3	3.0
Neutron (1)	3.04 ± 0.08	1.27 ± 0.05	9.6 ± 0.4 10.8 ± 0.6	
	3.10 ± 0.13		9.5	2.9

[1] Values are given as the mean ± standard deviation of a total of separate measurements as bracketted. For single runs, the standard deviation corresponds to that of the Guinier or $P(r)$ fits. The X-ray and neutron Q ranges used for Guinier fits is shown above each set of R_G and R_{XS} values. The L values correspond to the longest dimension of the macromolecule calculated as defined in section 2.

that of FVIIa. In other words, FVIIa and sTF form a side-by-side complex which leaves the overall length unchanged.

3.2. *Neutron data on factor VIIa, extracellular tissue factor and their complex*

Neutron scattering data were obtained for FVIIa, sTF and their complex in 100% ^2H_2O buffers. This corresponds to a negative solute-solvent contrast, compared to the positive contrast of the X-ray measurements [9,10]. The data served as a control of X-ray radiation damage (as no radiation effects occur with neutrons), and possible effects from large internal scattering density variations within FVIIa and the complex due to glycosylation. The Guinier analyses resulted in linear plots (Figs. 1 and 2). Values of c were 3.9–7.5 mg/ml for FVIIa, 0.9 mg/ml for sTF, and 2.6 mg/ml for the complex. No aggregation commonly observed with the use of ^2H_2O buffers was observed.

The corresponding sets of X-ray and neutron Guinier and $P(r)$ data in Table 1 generally showed good agreements with each other. This again demonstrated that the complex is intermediate in its structural anisotropy between those of FVIIa and sTF. Two exceptions to this agreement were the R_{XS} values for FVIIa and the complex, which were significantly reduced by neutrons compared to the X-ray values. This is attributed to the high electron density of carbohydrate relative to protein, which will cause the observed X-ray R_{XS} value to increase, and the neutron R_{XS} to decrease. Surface carbohydrate can have a large effect on solution scattering curves. Use of the average of the X-ray and neutron values will approximately represent a structure at infinite contrast by analogy with the Stuhrmann relationship, in which this contrast effect is minimised [9,10,25].

As the neutron intensities had been standardized using a deuterated polymer standard [23], the Guinier $I(0)/c$ values for FVIIa, sTF and their complex could be compared with $I(0)/c$ values for other proteins of known molecular weights. The $I(0)/c$ value for FVIIa and the complex were determined to be 0.051 and 0.072, respectively. The ratio of $I(0)/c$ values is 0.71:1.00, which is close to the ratio of 0.67:1.00 expected from the M_r values of 51,400 and 76,200. No calculation was made for sTF as c was too low for an accurate $I(0)/c$ value. Both $I(0)/c$ values were consistent with values of 0.093 for recombinant human IgE-Fc (M_r of 75,300) [22] and 0.181 for bovine IgG1 and IgG2 (M_r of 144,000) [24]. It is concluded that the complex was formed as expected.

4. Discussion

The solution scattering data show that FVIIa, sTF and their complex were monomeric, and that low resolution structural parameters can be derived from these. The X-ray and neutron data were self-consistent, and each data set served as a control of the other. Since the results can be averaged, the mean X-ray and neutron R_G values were computed from Table 1 to be 3.25 nm, 2.13 nm and 3.14 nm (± 0.13 nm) for FVIIa, sTF and their complex respectively. The mean R_{XS} values were 1.33 nm, 0.56 nm and 1.42 nm (± 0.13 nm), and the mean lengths L were

10.3 nm, 7.7 nm and 10.2 nm, respectively. Even though the molecular weights of FVIIa and sTF are comparable at 51,400 and 24,800, it is clearly seen that formation of the complex did not lead to significantly increased R_G or L values. These dimensions were very similar for FVIIa and the complex, indicating that the complex has a compact structure. This implies that many residues in both FVIIa and sTF will be in sufficiently close proximity to form intermolecular interactions to stabilise the complex. Both domains of sTF are expected to make such contacts with FVIIa, in agreement with the biochemical data [2], and there will be much scope for the design of anticoagulants that will prevent complex formation.

Fig. 4 indicates a schematic outline of the structures of the two free proteins and their mode of association in the complex as suggested from the scattering data. The interface between the EGF-2 and SP domains in the crystal structure of Factor Xa is defined by many contacts [5], and is presumed to be similar in FVIIa. The N- and C-terminal α-carbon atoms of the FVIIa Gla, EGF-1 and EGF-2 domains were arranged to lie on one linear axis. On this basis, the length of FVIIa in Fig. 4 is 10.2 nm, which agrees with the L values of Table 1, and suggests that the N-terminal domains of FVIIa are extended in solution. The length of sTF from the crystal structure is 8.3 nm, which also agrees with Table 1. The side-by-side model for the complex in Fig. 4 is consistent with biochemical data which show that a fragment of FVIIa containing both the Gla and EGF-1 domains inhibit complex formation [31]. Since the Gla domain of blood coagulation proteases is thought to bind to cell membranes, and full length tissue factor is associated with cell membranes via a C-terminal transmembrane region, it can be presumed that the two domains of sTF are aligned with the C-domain next to the Gla domain in the complex (Fig. 4). Ultimately the combination of the scattering curves in Figs. 1–3 with a recently-developed method of automated curve fitting of domain models to the scattering curves (which is constrained using known atomic structures for individual domains [22,24]) should permit the quantitative testing of sterically-allowed domain structures in FVIIa, sTF and their complex to produce improved low-resolution structures compared to those presented in Fig. 4.

Following completion of the present structural studies, a report has been made of a crystal structure of active site-inhibited FVIIa and a subtilisin-cleaved extracellular region of tissue factor [32]. This showed that a compact complex is formed with FVIIa and tissue factor positioned side-by-side, which is in good agreement with the scattering data.

Acknowledgements: A.W.A. and S.J.P. thank the BBSRC for grant support and the EPSRC for access to scattering cameras. D.J.D.J. and G.K.C. are supported by the MRC, and D.M.A.M. is supported by a MRC studentship. We thank Dr. W. Bras and Mrs. S. Slawson (SRS) and Dr. R.K. Heenan and Dr. S.M. King (ISIS) for generous instrumental support. We are indebted to Dr. D.L. Eaton of Genentech for the supply of crude sTF_{1-219} cell paste, and Dr. K. Harlos for the coordinates of sTF.

References

[1] Broze, G.J. (1994) In: Haemostasis and Thrombosis (Bloom, A.L., Forbes, C.D., Thomas, D.P. and Tuddenham, E.G.D., eds.) pp. 349–377, Churchill Livingstone, Edinburgh.
[2] Martin, D.M.A., Boys, C.W.G. and Ruf, W. (1995) FASEB J. 9, 852–859.
[3] Harlos, K., Martin, D.M A., O'Brien, D.P., Jones, E.Y., Stuart, D.I., Polikarpov, I., Miller, A., Tuddenham, E.G.D. and Boys, C.W.G.(1994) Nature 370, 662–666.
[4] Muller, Y.A., Ultsch, M.H., Kelley, R.F. and De Vos, A.M. (1994) Biochemistry, 33, 10864–10870.
[5] Padmanabhan, K., Padmanabhan, K.P., Tulinsky, A., Park, C.H., Bode, W., Huber, R., Blankenship, D.T., Cardin, A.D. and Kisiel, W. (1993) J. Mol. Biol. 232, 947–966.
[6] Baron, M., Norman, D.G., Harvey, T.S., Handford, P.A., Mayhew, M., Tse, A.G.D., Brownlee, G.G. and Campbell, I.D. (1992) Protein Sci. 1, 81–90.
[7] Selander, M., Persson, E., Stenflo, J. and Drakenberg, T. (1990) Biochemistry 29, 8111–8118.
[8] Soriano-Garcia, M., Padmanabhan, K., De Vos, A.M. and Tulinsky, A. (1992) Biochemistry 31, 2554–2566.
[9] Perkins, S.J. (1988) In: New Comprehensive Biochemistry (Neuberger, A. and Van Deenen, L.L.M., eds.) Vol. 11B Part II, pp. 143–264, Elsevier, Amsterdam.
[10] Perkins, S.J. (1994) In: Physical Methods of Analysis (Jones, C., Mulloy, B. and Thomas, A.H. eds.) Methods Mol. Biol. vol. 22, pp. 39–60. Humana Press Inc., New Jersey.
[11] Kemball-Cook, G., Garner, I., Imanaka, Y., Nishimura, T., O'Brien, D.P., Tuddenham, E.G.D and McVey, J.H. (1994) Gene 139, 275–279.
[12] O'Brien, D.P., Kemball-Cook, G., Hutchinson, A.M., Martin, D.M.A., Johnson, D.J.D., Byfield, P.G.H., Takamiya, O., Tuddenham, E.G.D. and McVey, J.H. (1994) Biochemistry 33, 14162–14169.
[13] Boys, C.W.G., Miller, A., Harlos, K., Martin, D.M.A., Tuddenham, E.G.D. and O'Brien, D.P. (1993) J. Mol. Biol. 234, 1263–1265.
[14] O'Brien, D.P., Gale, K.M., Anderson, S.J., McVey, J.H., Miller, G., Meade, T. and Tuddenham, E.G.D. (1991) Blood 78, 132–140.
[15] Perkins, S.J. (1986) Eur. J. Biochem. 157, 169–180.
[16] Hagen, F.S., Gray, C.L., O'Hara, P., Grant, F.J., Saari, G.C., Woodbury, R.G., Hart, C.E., Insley, M., Kisiel, W. and Kurachi, K. (1986) Proc. Natl. Acad. Sci. USA 83, 2412–2416.
[17] Fisher, K.L., Gorman, C.M., Vehar, G.A., O'Brien, D.P. and Lawn, R.M. (1987) Thromb. Res. 48, 89–99.
[18] Thim, L., Bjoern, S., Christensen, M., Nicolaisen, E.M., Lund-Hansen, T., Pedersen, A.H. and Hedner, U. (1988) Biochemistry, 27, 7785–7793.
[19] Harris, R.J. and Spellman, M.W. (1993) Glycobiology, 3, 219–224.
[20] Bjoern, S., Foster, D.C., Thim, L., Wiberg, F.C., Christensen, M., Komiyama, Y., Pedersen, A.H. and Kisiel, W. (1991) J. Biol. Chem. 266, 11051–11057.
[21] Towns-Andrews, E., Berry, A., Bordas, J., Mant, G.R., Murray, P.K., Roberts, K., Sumner, I., Worgan, J.S., Lewis, R. and Gabriel, A. (1989) Rev. Scient. Instrum. 60, 2346–2349.
[22] Beavil, A.J., Young, R.J., Sutton, B.J. and Perkins, S.J. (1995) Biochemistry, in press.
[23] Heenan, R.K. and King, S.M. (1993) Proceedings of an International Seminar on Structural Investigations at Pulsed Neutron Sources, Dubna, 1st-4th September 1992. Report E3-93-65. Joint Institute for Nuclear Research, Dubna.
[24] Mayans, M.O., Coadwell, W.J., Beale, D., Symons, D.B.A. and Perkins, S.J. (1995) Biochem. J. 311, 283–291.
[25] Glatter, O. and Kratky, O. (eds.) (1982) Small-angle X-ray scattering, Academic Press, New York.
[26] Kratky, O. (1963) Progr. Biophys. Chem. 13, 105–173.
[27] Hjelm, R.J. (1985) J. Appl. Crystallogr. 18, 452–460.
[28] Perkins, S.J., Chung, L.P. and Reid, K.B.M. (1986) Biochem. J. 223, 779–807.
[29] Svergun, D.I., Semenyuk, A.V. and Feigin, L.A. (1988) Acta Crystallogr. A44, 244–250.
[30] Waxman, E., Laws, W.R., Laue, T.M., Nemerson, Y. and Ross, J.B.A. (1993) Biochemistry 32, 3005–3012.
[31] Kazama, Y., Pastuszin, A., Wildgoose, P., Hamamoto, T. and Kisiel, W. (1993) J. Biol. Chem. 268, 16231–16240.
[32] Banner, D.W., D'Arcy, A., Chene, C., Vilbois, F., Konigsberg, W.H., Guha, A., Nemerson, Y. and Kirchofer, D. (1995) Thromb. Haemostas. 73, 1183 (abstract).